# Noninvasive imaging of the human rod photoreceptor mosaic using a confocal adaptive optics scanning ophthalmoscope

**Alfredo Dubra,[1,2,*] Yusufu Sulai,[3] Jennifer L. Norris,[2] Robert F. Cooper,[4] Adam M. Dubis,[5] David R. Williams,[2] and Joseph Carroll[5,6,7]**

[1]*Flaum Eye Institute, University of Rochester, Rochester, NY 14642, USA*
[2]*Center for Visual Science, University of Rochester, Rochester, NY 14627, USA*
[3]*The Institute of Optics, University of Rochester, Rochester, NY 14627, USA*
[4]*Department of Biomedical Engineering, Marquette University, Milwaukee, WI 53223, USA*
[5]*Department of Cell Biology, Neurobiology & Anatomy, Medical College of Wisconsin, Milwaukee, WI 53226, USA*
[6]*Department of Ophthalmology, Medical College of Wisconsin, Milwaukee, WI 53226, USA*
[7]*Department of Biophysics, Medical College of Wisconsin, Milwaukee, WI 53226, USA*
**adubra@cvs.rochester.edu*

**Abstract:** The rod photoreceptors are implicated in a number of devastating retinal diseases. However, routine imaging of these cells has remained elusive, even with the advent of adaptive optics imaging. Here, we present the first *in vivo* images of the contiguous rod photoreceptor mosaic in nine healthy human subjects. The images were collected with three different confocal adaptive optics scanning ophthalmoscopes at two different institutions, using 680 and 775 nm superluminescent diodes for illumination. Estimates of photoreceptor density and rod:cone ratios in the 5°–15° retinal eccentricity range are consistent with histological findings, confirming our ability to resolve the rod mosaic by averaging multiple registered images, without the need for additional image processing. In one subject, we were able to identify the emergence of the first rods at approximately 190 μm from the foveal center, in agreement with previous histological studies. The rod and cone photoreceptor mosaics appear in focus at different retinal depths, with the rod mosaic best focus (i.e., brightest and sharpest) being at least 10 μm shallower than the cones at retinal eccentricities larger than 8°. This study represents an important step in bringing high-resolution imaging to bear on the study of rod disorders.

© 2011 Optical Society of America

**OCIS codes:** (110.1080) Active or adaptive optics; (330.5310) Vision—photoreceptors; (170.1610) Clinical applications; (170.3880) Medical and biological imaging; (170.4470) Ophthalmology.

## References and links

1. C. A. Curcio, K. R. Sloan, R. E. Kalina, and A. E. Hendrickson, "Human photoreceptor topography," J. Comp. Neurol. **292**(4), 497–523 (1990).
2. E. L. Berson, "Retinitis pigmentosa. The Friedenwald Lecture," Invest. Ophthalmol. Vis. Sci. **34**(5), 1659–1676 (1993).
3. K. R. Alexander and G. A. Fishman, "Prolonged rod dark adaptation in retinitis pigmentosa," Br. J. Ophthalmol. **68**(8), 561–569 (1984).
4. C. P. Hamel, "Cone rod dystrophies," Orphanet J. Rare Dis. **2**(1), 7 (2007).
5. M. Michaelides, A. J. Hardcastle, D. M. Hunt, and A. T. Moore, "Progressive cone and cone-rod dystrophies: phenotypes and underlying molecular genetic basis," Surv. Ophthalmol. **51**(3), 232–258 (2006).
6. Y. Miyake, K. Yagasaki, M. Horiguchi, Y. Kawase, and T. Kanda, "Congenital stationary night blindness with negative electroretinogram. A new classification," Arch. Ophthalmol. **104**(7), 1013–1020 (1986).
7. C. A. Curcio, C. Owsley, and G. R. Jackson, "Spare the rods, save the cones in aging and age-related maculopathy," Invest. Ophthalmol. Vis. Sci. **41**(8), 2015–2018 (2000).
8. C. A. Curcio, N. E. Medeiros, and C. L. Millican, "Photoreceptor loss in age-related macular degeneration," Invest. Ophthalmol. Vis. Sci. **37**(7), 1236–1249 (1996).
9. R. Adler, C. Curcio, D. Hicks, D. Price, and F. Wong, "Cell death in age-related macular degeneration," Mol. Vis. **5**, 31 (1999).

#145204 - $15.00 USD Received 1 Apr 2011; revised 2 Jun 2011; accepted 3 Jun 2011; published 8 Jun 2011
(C) 2011 OSA

10. K. R. Kendell, H. A. Quigley, L. A. Kerrigan, M. E. Pease, and E. N. Quigley, "Primary open-angle glaucoma is not associated with photoreceptor loss," Invest. Ophthalmol. Vis. Sci. **36**(1), 200–205 (1995).
11. T. M. Nork, J. N. Ver Hoeve, G. L. Poulsen, R. W. Nickells, M. D. Davis, A. J. Weber, S. H. Vaegan, S. H. Sarks, H. L. Lemley, and L. L. Millecchia, "Swelling and loss of photoreceptors in chronic human and experimental glaucomas," Arch. Ophthalmol. **118**(2), 235–245 (2000).
12. H. Gao and J. G. Hollyfield, "Aging of the human retina. Differential loss of neurons and retinal pigment epithelial cells," Invest. Ophthalmol. Vis. Sci. **33**(1), 1–17 (1992).
13. C. A. Curcio, C. L. Millican, K. A. Allen, and R. E. Kalina, "Aging of the human photoreceptor mosaic: evidence for selective vulnerability of rods in central retina," Invest. Ophthalmol. Vis. Sci. **34**(12), 3278–3296 (1993).
14. J. Liang, D. R. Williams, and D. T. Miller, "Supernormal vision and high-resolution retinal imaging through adaptive optics," J. Opt. Soc. Am. A **14**(11), 2884–2892 (1997).
15. A. Roorda and D. R. Williams, "The arrangement of the three cone classes in the living human eye," Nature **397**(6719), 520–522 (1999).
16. A. Roorda, A. B. Metha, P. Lennie, and D. R. Williams, "Packing arrangement of the three cone classes in primate retina," Vision Res. **41**(10-11), 1291–1306 (2001).
17. A. Roorda and D. R. Williams, "Optical fiber properties of individual human cones," J. Vis. **2**(5), 4 (2002).
18. J. Carroll, M. Neitz, H. Hofer, J. Neitz, and D. R. Williams, "Functional photoreceptor loss revealed with adaptive optics: an alternate cause of color blindness," Proc. Natl. Acad. Sci. U.S.A. **101**(22), 8461–8466 (2004).
19. J. I. Wolfing, M. Chung, J. Carroll, A. Roorda, and D. R. Williams, "High-resolution retinal imaging of cone-rod dystrophy," Ophthalmology **113**(6), 1014–1019.e1 (2006).
20. S. S. Choi, N. Doble, J. L. Hardy, S. M. Jones, J. L. Keltner, S. S. Olivier, and J. S. Werner, "*In vivo* imaging of the photoreceptor mosaic in retinal dystrophies and correlations with visual function," Invest. Ophthalmol. Vis. Sci. **47**(5), 2080–2092 (2006).
21. J. L. Duncan, Y. Zhang, J. Gandhi, C. Nakanishi, M. Othman, K. E. H. Branham, A. Swaroop, and A. Roorda, "High-resolution imaging with adaptive optics in patients with inherited retinal degeneration," Invest. Ophthalmol. Vis. Sci. **48**(7), 3283–3291 (2007).
22. A. Roorda, Y. Zhang, and J. L. Duncan, "High-resolution *in vivo* imaging of the RPE mosaic in eyes with retinal disease," Invest. Ophthalmol. Vis. Sci. **48**(5), 2297–2303 (2007).
23. R. C. Baraas, J. Carroll, K. L. Gunther, M. Chung, D. R. Williams, D. H. Foster, and M. Neitz, "Adaptive optics retinal imaging reveals S-cone dystrophy in tritan color-vision deficiency," J. Opt. Soc. Am. A **24**(5), 1438–1447 (2007).
24. K. Grieve and A. Roorda, "Intrinsic signals from human cone photoreceptors," Invest. Ophthalmol. Vis. Sci. **49**(2), 713–719 (2008).
25. T. Y. Chui, H. Song, and S. A. Burns, "Adaptive-optics imaging of human cone photoreceptor distribution," J. Opt. Soc. Am. A **25**(12), 3021–3029 (2008).
26. M. K. Yoon, A. Roorda, Y. Zhang, C. Nakanishi, L. J. Wong, Q. Zhang, L. Gillum, A. Green, and J. L. Duncan, "Adaptive optics scanning laser ophthalmoscopy images in a family with the mitochondrial DNA T8993C mutation," Invest. Ophthalmol. Vis. Sci. **50**(4), 1838–1847 (2009).
27. C. Torti, B. Považay, B. Hofer, A. Unterhuber, J. Carroll, P. K. Ahnelt, and W. Drexler, "Adaptive optics optical coherence tomography at 120,000 depth scans/s for non-invasive cellular phenotyping of the living human retina," Opt. Express **17**(22), 19382–19400 (2009).
28. R. J. Zawadzki, B. Cense, Y. Zhang, S. S. Choi, D. T. Miller, and J. S. Werner, "Ultrahigh-resolution optical coherence tomography with monochromatic and chromatic aberration correction," Opt. Express **16**(11), 8126–8143 (2008).
29. O. P. Kocaoglu, S. Lee, R. S. Jonnal, Q. Wang, A. E. Herde, J. C. Derby, W. Gao, and D. T. Miller, "Imaging cone photoreceptors in three dimensions and in time using ultrahigh resolution optical coherence tomography with adaptive optics," Biomed. Opt. Express **2**(4), 748–763 (2011).
30. J. T. McAllister, A. M. Dubis, D. M. Tait, S. Ostler, J. Rha, K. E. Stepien, C. G. Summers, and J. Carroll, "Arrested development: high-resolution imaging of foveal morphology in albinism," Vision Res. **50**(8), 810–817 (2010).
31. R. S. Jonnal, J. R. Besecker, J. C. Derby, O. P. Kocaoglu, B. Cense, W. Gao, Q. Wang, and D. T. Miller, "Imaging outer segment renewal in living human cone photoreceptors," Opt. Express **18**(5), 5257–5270 (2010).
32. J. Carroll, E. Banin, D. M. Hunt, R. Martin, M. Michaelides, L. Mizrahi-Meissonnier, A. T. Moore, D. Sharon, D. R. Williams and A. Dubra, "Evaluating the photoreceptor mosaic in blue cone monochromacy (BCM)," Invest. Ophthalmol. Vis. Sci. **51**, E-Abstract 2935 (2010).
33. J. Carroll, S. S. Choi, and D. R. Williams, "*In vivo* imaging of the photoreceptor mosaic of a rod monochromat," Vision Res. **48**(26), 2564–2568 (2008).
34. N. Doble, S. S. Choi, J. L. Codona, J. Christou, J. M. Enoch, and D. R. Williams, "*In vivo* imaging of the human rod photoreceptor mosaic," Opt. Lett. **36**(1), 31–33 (2011).
35. M. Alpern, C. C. Ching, and K. Kitahara, "The directional sensitivity of retinal rods," J. Physiol. **343**, 577–592 (1983).
36. J. A. Van Loo, Jr., and J. M. Enoch, "The scotopic Stiles-Crawford effect," Vision Res. **15**(8-9), 1005–1009 (1975).
37. A. Dubra and Y. Sulai, "The reflective afocal broadband adaptive optics scanning ophthalmoscope," Biomed. Opt. Express **2**(6), 1757–1768 (2011).
38. A. Dubra and Z. Harvey, "Registration of 2D Images from Fast Scanning Ophthalmic Instruments," in *Biomedical Image Registration*, Vol. 6204 of Lecture Notes in Computer Science (Springer, Berlin), pp. 60–71 (2010).

#145204 - $15.00 USD Received 1 Apr 2011; revised 2 Jun 2011; accepted 3 Jun 2011; published 8 Jun 2011
(C) 2011 OSA

39. ANSI, "American National Standard for safe use of lasers (ANSI 136.1)," ANSI 136.1–2007 (The Laser Institute of America, 2007).
40. F. C. Delori, R. H. Webb, and D. H. Sliney; American National Standards Institute, "Maximum permissible exposures for ocular safety (ANSI 2000), with emphasis on ophthalmic devices," J. Opt. Soc. Am. A **24**(5), 1250–1265 (2007).
41. C. W. Oyster, *The Human Eye: Structure and Function* (Sinauer Associates Inc, Sunderland, Massachusetts, 1999).
42. L. N. Thibos, M. Ye, X. Zhang, and A. Bradley, "The chromatic eye: a new reduced-eye model of ocular chromatic aberration in humans," Appl. Opt. **31**(19), 3594–3600 (1992).
43. K. Y. Li and A. Roorda, "Automated identification of cone photoreceptors in adaptive optics retinal images," J. Opt. Soc. Am. A **24**(5), 1358–1363 (2007).
44. J. Carroll, R. C. Baraas, M. Wagner-Schuman, J. Rha, C. A. Siebe, C. Sloan, D. M. Tait, S. Thompson, J. I. W. Morgan, J. Neitz, D. R. Williams, D. H. Foster, and M. Neitz, "Cone photoreceptor mosaic disruption associated with Cys203Arg mutation in the M-cone opsin," Proc. Natl. Acad. Sci. U.S.A. **106**(49), 20948–20953 (2009).
45. O. S. Packer, D. R. Williams, and D. G. Bensinger, "Photopigment transmittance imaging of the primate photoreceptor mosaic," J. Neurosci. **16**(7), 2251–2260 (1996).
46. A. Pallikaris, D. R. Williams, and H. Hofer, "The reflectance of single cones in the living human eye," Invest. Ophthalmol. Vis. Sci. **44**(10), 4580–4592 (2003).
47. C. A. Curcio and K. R. Sloan, "Packing geometry of human cone photoreceptors: variation with eccentricity and evidence for local anisotropy," Vis. Neurosci. **9**(02), 169–180 (1992).
48. D. Pum, P. K. Ahnelt, and M. Grasl, "Iso-orientation areas in the foveal cone mosaic," Vis. Neurosci. **5**(06), 511–523 (1990).
49. D. R. Williams, "Topography of the foveal cone mosaic in the living human eye," Vision Res. **28**(3), 433–454 (1988).
50. T. Wilson and A. R. Carlini, "Size of the detector in confocal imaging systems," Opt. Lett. **12**(4), 227–229 (1987).
51. J. Carroll, E. A. Rossi, J. Porter, J. Neitz, A. Roorda, D. R. Williams, and M. Neitz, "Deletion of the X-linked opsin gene array locus control region (LCR) results in disruption of the cone mosaic," Vision Res. **50**(19), 1989–1999 (2010).
52. S. B. Stevenson and A. Roorda, "Correcting for miniature eye movements in high resolution scanning laser ophthalmoscopy," Proc. SPIE **5688A**, 145–151 (2005).
53. D. W. Arathorn, Q. Yang, C. R. Vogel, Y. Zhang, P. Tiruveedhula, and A. Roorda, "Retinally stabilized cone-targeted stimulus delivery," Opt. Express **15**(21), 13731–13744 (2007).
54. J. Porter, College of Optometry, University of Houston, 4901 Calhoun Rd, Houston, TX 77204–2020 (personal communication, 2010).
55. D. Merino, University of California San Francisco Medical Center, 400 Parnassus Ave, San Francisco, CA 94143–0344 (personal communication, 2010).

## 1. Introduction

The human photoreceptor mosaic is multifaceted—among other things, providing exquisite resolution of spatial detail, single-photon sensitivity, and discrimination of millions of hues. These functional capabilities are a result of the presence of two interleaved mosaics of photoreceptors : rods and cones. Despite the majority of our daily vision being driven by the cone photoreceptors, nearly 95% of the total photoreceptor population in the human retina comprises rods [1]. Rod dysfunction is involved in a variety of devastating retinal degenerations, including retinitis pigmentosa [2,3], cone-rod dystrophy [4,5], congenital stationary night blindness [6], age-related macular degeneration [7–9], and more controversially in glaucoma [10,11]. Moreover, the rods are thought to be preferentially compromised in normal aging [12,13]. Currently lacking are tools with which to assess rod structure in the living retina; such tools could enable researchers to elucidate the sequence of events that ultimately lead to vision loss in these conditions, as well as allow for improved monitoring of the efficacy of current and new treatments.

Since the introduction of adaptive optics (AO) technology to ophthalmic imaging [14], individual cone photoreceptors, retinal pigment epithelial (RPE) cells, and white blood cells have been routinely imaged by a number of investigators (e.g., [15–31]). However, despite rods outnumbering cones by 20:1, they have resisted visualization with these same imaging devices. There are only a few reports of rods being imaged in the diseased retina [32,33], and the single report of rod visualization in the normal retina relied on significant image processing and enhancement, and resulted in only intermittent rod visualization [34]. This has been thought to be due to their small size and/or their reduced waveguide capabilities [35,36].

#145204 - $15.00 USD Received 1 Apr 2011; revised 2 Jun 2011; accepted 3 Jun 2011; published 8 Jun 2011
(C) 2011 OSA

Here we demonstrate the first images of the contiguous rod photoreceptor mosaic in a series of normal subjects, obtained using adaptive optics scanning ophthalmoscopes (AOSOs). The complete rod mosaic is visible even in some individual AOSO frames. These results argue against a fundamental barrier to imaging rods *in vivo*, provided the optical system [37] and image registration software [38] are sufficiently optimized. These findings open the door for examining rod involvement in retinal disease using AO imaging, as has been done for eye conditions involving the cone photoreceptors [18–21,23,26,27].

## 2. Methods

Written informed consent was obtained after the nature and possible risks of the imaging study were explained to the subjects. Studies were approved by Institutional Review Boards at the University of Rochester and the Medical College of Wisconsin. The eye to be imaged was dilated and cycloplegia was induced with topical application of one drop of a combination of phenylephrine hydrochloride (2.5%) and tropicamide (1%). The subjects were aligned and stabilized with the use of a dental impression on a bite bar. The light exposure was kept below the safe use of laser ANSI standard maximum permissible exposure [39,40] at all times. Reflectance images were recorded using three AOSOs as described in [37], with one of them having slightly different folding angles in the reflective afocal telescopes due to mechanical constraints imposed by off-the-shelf mounts for the optical elements. The use of multiple AOSOs with different pinhole sizes in front of the detectors and different angles of incidence on the spherical mirrors, allowed us to test the robustness of the minimization of astigmatism in planes conjugate to the pupil of the eye and the retina simultaneously [37].

Two superluminescent diodes (SLDs) with peak wavelengths 680 and 775 nm were used for imaging, with 8.5 and 13.7 nm full-width at half-maximum (FWHM) bandwidths, respectively. The SLDs were from Superlum Ireland (Carrigtwohill, County Cork, Ireland) and Inphenix Inc. (Livermore, California, USA), respectively. Confocal pinholes of 0.4, 0.6, 1.1, or 1.5 Airy disks in diameter were used to spatially filter the scattered light from out-of-focus retinal layers before the detector.

The axial lengths of the eyes imaged were measured by using an IOL Master (Carl Zeiss Meditec, Inc., Dublin, California, USA), and are provided in Table 1, along with other relevant information. Eight of the nine subjects were emmetropic, and the remaining subject, DLAB_0003, was a mild myope (~1.0 D). While, theoretically, an eye with a shorter axial length would provide better resolution, it should be noted that the mean axial length of our subjects (23.8 mm) was comparable with that reported for a large normal population (24 mm) [41].

For an eye with a 17 mm effective focal length and a pupil diameter larger than the beam diameter entering the eye (7.5 mm), the lateral resolution (Rayleigh criterion) is 1.4 μm for 680 nm light and 1.6 μm for 775 nm. Under the same assumptions, the corresponding axial resolution values are 15 and 17 μm. These numbers are optimistic (i.e., small) if we keep in mind the nonzero bandwidth of the light sources and the significant longitudinal chromatic aberration of the eye [42].

Sequences of 50–200 images were recorded, using between 0.75° and 1.00° fields-of-view. The image stretching resulting from the sinusoidal motion of the resonant optical scanner was compensated by estimating the distortion from images of a Ronchi ruling and then resampling the images over a grid of equally spaced pixels. To increase the signal-to-noise ratio, eye motion artifacts were removed, and then a number of registered frames were averaged [38]. In what follows, unless otherwise stated, all the *in vivo* photoreceptor images correspond to registered averages of multiple raw frames. No additional image processing or filtering techniques have been applied to any of the images analyzed in this study or shown in any of the figures. Because of the large spatial variation observed in photoreceptor brightness and for display purposes only, the images are displayed using both a linear and a logarithmic gray scale mapping [37].

#145204 - $15.00 USD Received 1 Apr 2011; revised 2 Jun 2011; accepted 3 Jun 2011; published 8 Jun 2011
(C) 2011 OSA

**Table 1. Axial Lengths and Retinal Locations Imaged in this Study for Cell Density Estimation**

| Subject | Gender | Age (years) | Eye[a] | Axial length (mm) | Retinal location (deg)[b] | Instrument[c] |
|---|---|---|---|---|---|---|
| WLAB001 | Male | 28 | OS | 22.83 | 8, 10, 15 | ROC 1 |
| WLAB002 | Male | 29 | OD | 23.23 | 5, 10, 15 | ROC 1 |
| DLAB_0003 | Male | 24 | OS | 24.32 | 10, 15 | ROC 2 |
| DLAB_0007 | Male | 30 | OS | 23.59 | 5, 10, 15 | ROC 2 |
| DLAB_0008 | Male | 21 | OS | 24.44 | 5, 10, 15 | ROC 2 |
| DLAB_0009 | Male | 27 | OS | 24.64 | 5, 10 | ROC 2 |
| JC_0565 | Female | 31 | OS | 24.01 | 10 | MKE 1 |
| JC_0002 | Male | 27 | OD | 24.72 | 10 | MKE 1 |
| JC_0138 | Female | 27 | OD | 22.75 | 10 | MKE 1 |

[a]OD corresponds to right eye and OS to left eye.
[b]Locations are all temporal eccentricity, relative to fixation.
[c]ROC indicates University of Rochester and MKE the Medical College of Wisconsin.

Estimates of cell density were obtained by counting the number of rods (or cones) within a given image patch of known area. The location of individual rods and cones was identified by using an automated algorithm, which also allowed manual addition/subtraction of cones or rods missed or selected in error by the algorithm [43,44]. Mosaic regularity and packing geometry was assessed by using previously described Voronoi analyses [23,44]. The relative retinal location of each image was determined based on the predetermined fixation location. In three subjects, the position based on fixation was further refined by using blood vessels as landmarks.

## 3. Results and discussion

Images of the full and contiguous photoreceptor mosaic at retinal locations between 5° and 15° temporal to the fovea along the horizontal meridian were recorded in 9 healthy human subjects. Foveal fixation was confirmed by examining the appearance of the cone mosaic while the subject was fixating at the center of the raster scan (data not shown). This eccentricity range spans from a cone-dominated to a rod-dominated location in terms of area, as shown in Fig. 1 below. Note that most of the rod photoreceptor mosaic can be resolved in the logarithmic image, despite the 80% increase in the FWHM of the PSF with respect to the image displayed with a linear grayscale.

Notably, the transmission images recorded by Packer *et al.* [45] (see Figs. 2a and 2b) resemble the *in vivo* images (e.g., Figure 2c). The bright spots in the histological images correspond to light guided by both rod and cone photoreceptor outer segments. In both our images and those by Packer *et al*., the area around the central bright spot of each cone typically appears as a dark ring, which represents the boundary of its inner segment.

The images in Fig. 3 illustrate how averaging multiple registered frames reduces the photon and readout noise that gives single raw frames a grainy appearance. The optimal number of images to average depends on the inherent eye motion, signal-to-noise ratio (SNR) of each particular image series, the image registration algorithm, and the AO correction, among other factors. Three regimes can be observed, depending on the number of images averaged. First, when the number of images is low, assuming perfect image registration and AO correction, the image quality would be limited by readout, photon, or background (i.e., stray light) noise. Second, if the number of averaged images is adequate, and provided the image registration is acceptable, diffraction or residual aberrations would limit the image resolution. Third, when the number of images is too high, the accumulation of imperfectly registered images would blur the average of registered images, and thus the resolution would be limited by the registration algorithm itself. Determining what is an “acceptable” or the

#145204 - $15.00 USD Received 1 Apr 2011; revised 2 Jun 2011; accepted 3 Jun 2011; published 8 Jun 2011
(C) 2011 OSA

"optimal" number of images is by no means trivial, and any attempt to obtain a "rule of thumb" is complicated by tear film disruption, intraocular scattering, residual accommodation, pupil diameter, and other experimental factors. Interestingly, averaging images collected at different times during the day reduces the large cell differences in rod (and cone) reflectivity across the mosaic, as illustrated by the images in Fig. 3. In addition, the uniformity of the reflectivity profile of certain cells also becomes more uniform as a result of averaging images from different time points [46].

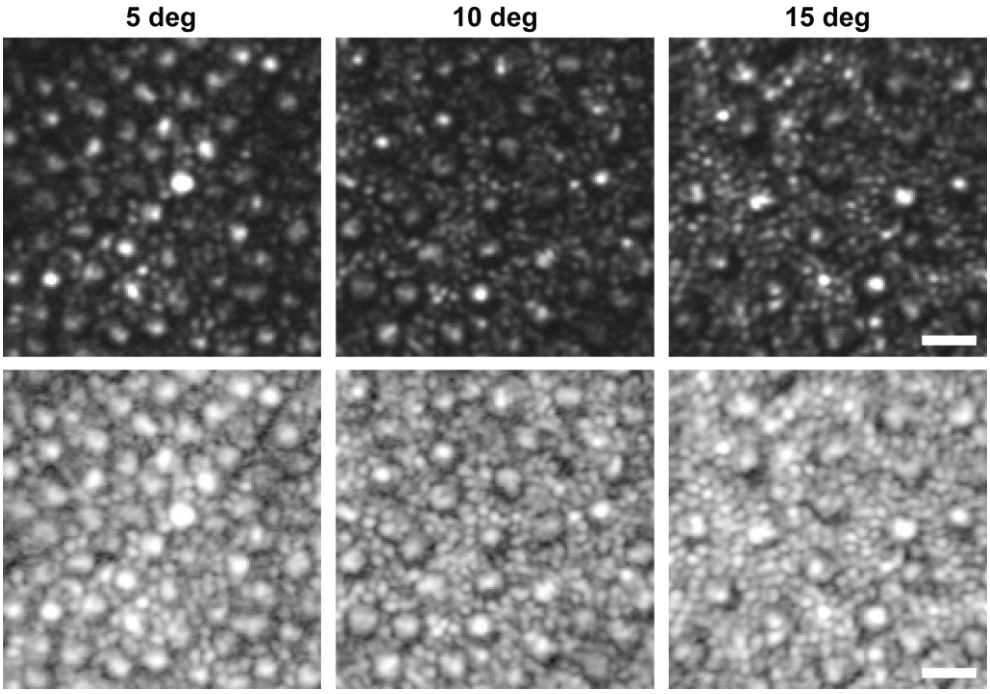


Fig. 1. Reflectance images of the human photoreceptor mosaic at three retinal locations along the temporal meridian for subject DLAB_0008, collected using 680 nm light and 0.4 Airy disk pinhole size. The same images are shown with linear (*top row*) and logarithmic (*bottom row*) grayscales, to facilitate visualization of the rod mosaic. The scale bars are 10 μm across.

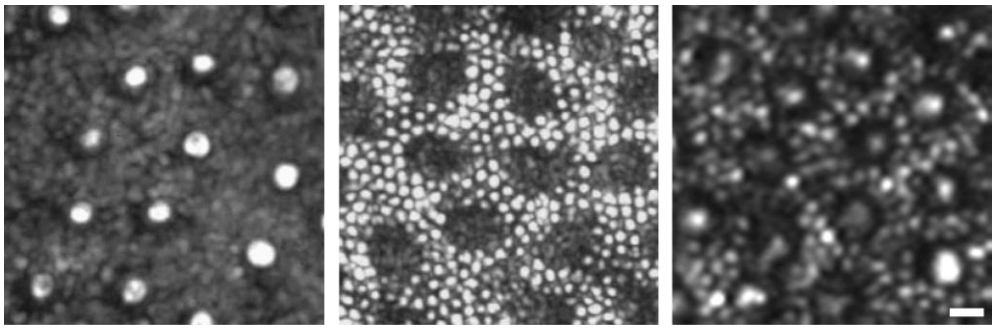

Fig. 2. The two images on the left and middle were collected in an excised primate retina, imaged in a bright field microscope in transmission [45]. These images, reproduced with permission from the Journal of Neuroscience, show the cone and rod outer segment tips, respectively, as bright spots. The image on the right shows an *in vivo* image from WLAB001 at similar eccentricity, collected using 775 nm light and 0.6 Airy disk pinhole size. The scale bar is 5 μm across.

#145204 - $15.00 USD Received 1 Apr 2011; revised 2 Jun 2011; accepted 3 Jun 2011; published 8 Jun 2011
(C) 2011 OSA

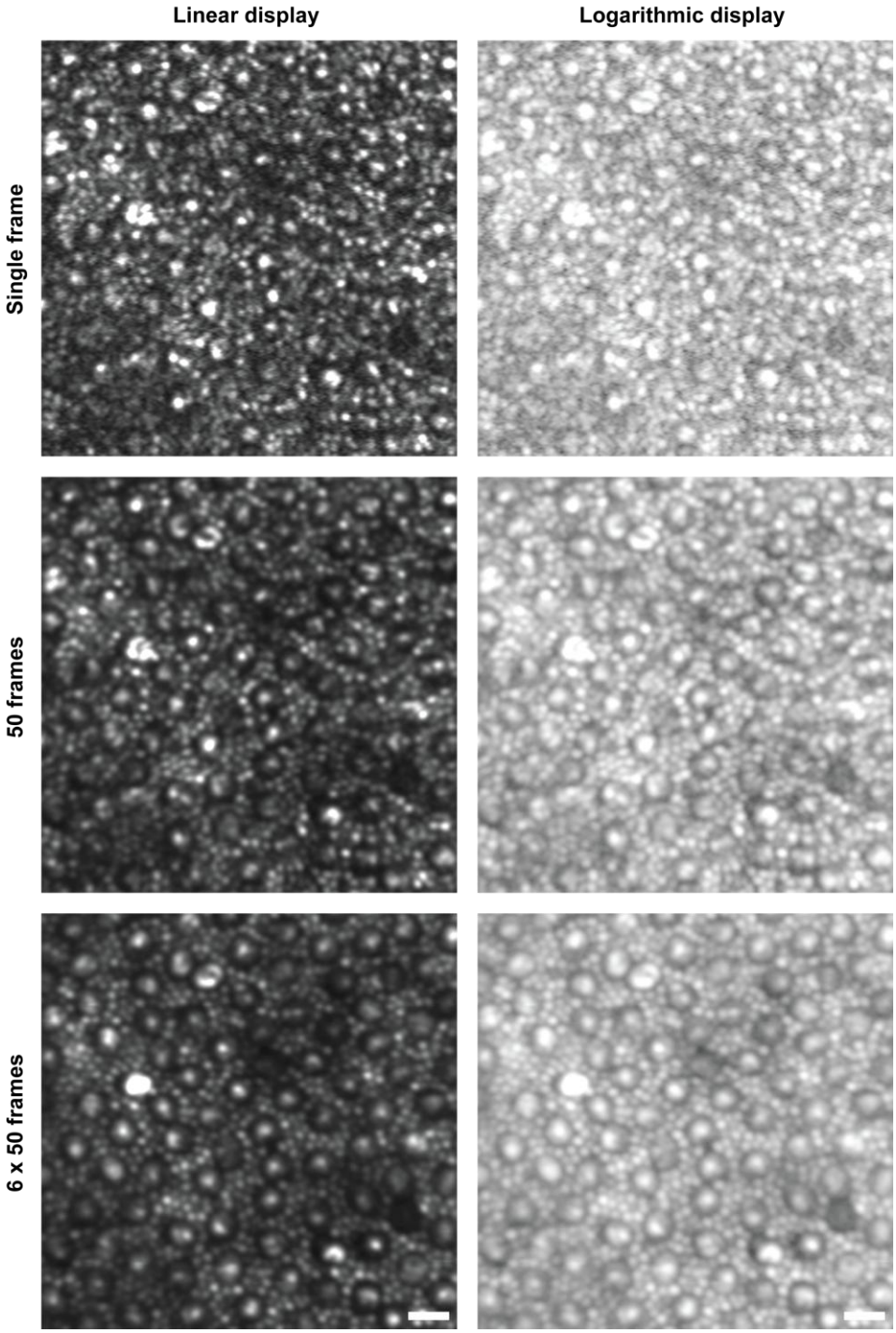


Fig. 3. Reflectance images of the human photoreceptor mosaic at 10° temporal to the fovea for subject JC_0138, collected using 680 nm light and 1.1 Airy disk pinhole size. From top to bottom the images are: a single frame, a registered average of 50 frames, and registered average of 6 batches of 50 frames, collected over a 6 hour period, 1 hour apart. The scale bars are 20 μm across.

#145204 - $15.00 USD Received 1 Apr 2011; revised 2 Jun 2011; accepted 3 Jun 2011; published 8 Jun 2011
(C) 2011 OSA

While the images shown here demonstrate the ability to resolve the rod photoreceptor mosaic, the clinical utility of these images ultimately requires extraction of quantitative information. Shown in Fig. 4 are rod:cone ratio and cell density measurements for all 9 subjects. The estimated values are in reasonable agreement with the histological findings from Curcio *et al.* [1], even at the point of maximum rod density. The small difference between our values and those obtained via histological analysis are likely due to inter-subject variability. Other sources of discrepancy could be errors in determining the retinal location, not accounting for shorter axial lengths at eccentric locations, or even tissue shrinkage artifacts in the histological data. Regardless, these data represent the first *in vivo* estimates of rod photoreceptor density in the normal retina. The fact that the rod mosaic can be fully resolved in young people is encouraging in terms of studying advanced stages of eye disease in older patients. While imaging of older subjects would be expected to result in images of lower resolution due to the opacification of the intraocular media and smaller pupil size, the loss and enlargement of rod photoreceptors observed in the aging retina [12,13] might partially compensate for this resolution loss.

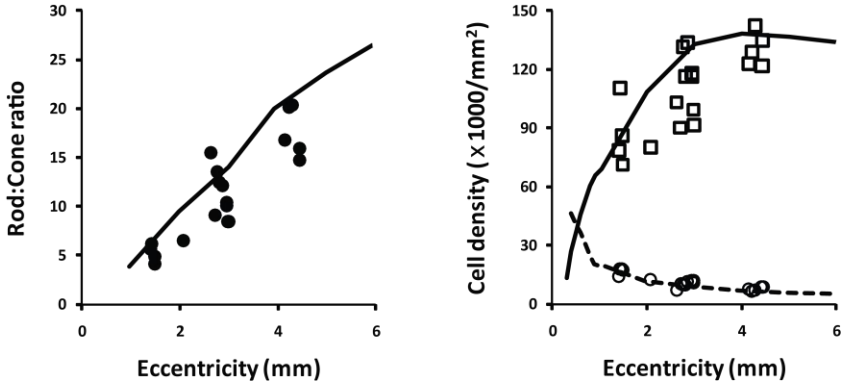


Fig. 4. Comparison of *in vivo* rod and cone metrics with those from Curcio *et al*. [1]. Shown on the left is a plot of the ratio of rods to cones as a function of retinal eccentricity. The solid line is the mean of Curcio's measurements taken in the temporal meridian, and filled circles correspond to the data from this study. On the right is a plot of photoreceptor density as a function of retinal eccentricity. Density estimates for our subjects for rods and cones are shown as open squares and open circles, respectively. Also plotted is the mean rod (*solid line*) and cone (*dashed line*) density values reported by Curcio *et al.* [1] for the temporal meridian.

With the ability to resolve the complete peripheral photoreceptor mosaic, we sought to investigate the spatial organization of the interleaved rod and cone mosaics. The normal foveal and parafoveal cone mosaic has been well described as being triangular (hexagonally packed) both in histological [47–49] and more recently, using *in vivo* imaging tools [25,43]. Given the normal variation in cone density, these metrics have also been employed to examine disruptions in mosaic regularity caused by retinal disease [21,23,51]. Shown in Fig. 5 is a Voronoi representation of an image of the photoreceptor mosaic taken at 10° temporal to the fovea. Nearly all the cones in the image have more than 8 rods surrounding them (red and dark blue cells in panel b). When examining only the cones, we see that 48% of them have six-sided Voronoi domains (green cells, panel c), indicating that even at this location, the cone mosaic is roughly organized in a triangular lattice. However, this is reduced in comparison to the parafoveal mosaic, which has been reported to have as many as 60%–70% of cones in a given patch of retina having six-sided Voronoi domains [23,25]. We find that at this eccentricity, the rods are similarly packed, with 48% of the rods having six-sided Voronoi domains. Of course, since at this location only a minority of the rods do not have a cone as an immediately adjacent neighbor, it is difficult to assess the packing geometry of the isolated rod mosaic without incorporating the disruptive effect of the interleaved cone mosaic. Further work is needed to assess the normal geometry of the rod mosaic in the context of the cone mosaic.

#145204 - $15.00 USD Received 1 Apr 2011; revised 2 Jun 2011; accepted 3 Jun 2011; published 8 Jun 2011
(C) 2011 OSA

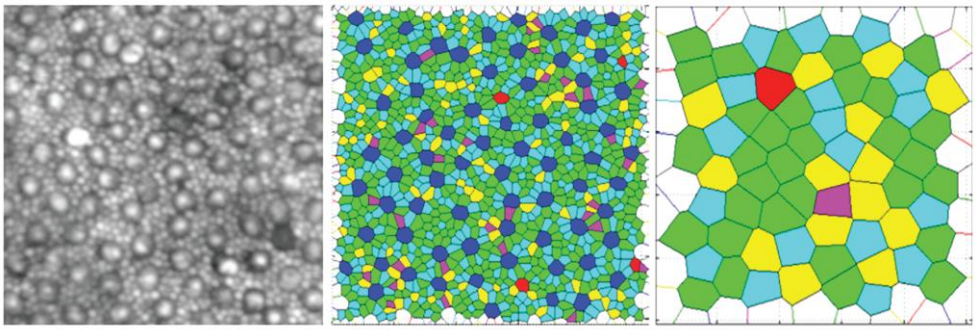


Fig. 5. Analysis of the regularity of the peripheral photoreceptor mosaic. Shown in a is the 6-hour averaged image (logarithmic display) from subject JC_0138, taken at about 10° temporal to fixation, collected using 680 nm light and 1.1 Airy disk pinhole size. Color-coded Voronoi domains associated with each cell are shown in panel b), where the color indicates the number of sides on each Voronoi polygon (magenta = 4, cyan = 5, green = 6, yellow = 7, red = 8, dark blue = 9). Regions of six-sided polygons indicate a regular triangular lattice, while other color mark points of disruption of the mosaic. Panel c shows the color-coded Voronoi domains associated with just the cone photoreceptors in the image.

Another well-known feature of the human rod mosaic is the existence of a rod-free zone at the center of the fovea. The resolution of our AOSOs also enables visualization of this anatomical feature of the rod mosaic. Images of the parafoveal photoreceptor mosaic show rod photoreceptors as close as 190 μm away from the foveal center (Fig. 6). This is consistent with previous *ex vivo* data, in which rod photoreceptors were found to first appear between 100 and 200 μm from the foveal center [1], and also with *in vivo* AO imaging of blue cone monochromacy, which enabled direct visualization of both the rod free zone and S-cone free zone of the human fovea [32].

Critical to successful visualization of the rod mosaic is correct focusing of the AOSO. The sequence of images in Fig. 7 shows that even though many rods can be resolved over the 35 μm range covered by the sequence, the full mosaic can only be reliably resolved in one of the images (8.7 μm). This suggests that the coarsest focus step used to image the rod mosaic using 680 nm light should be no larger than 10 μm.

Across all subjects, we find that the cones and rods do not necessarily appear in focus at the same time, with the rods appearing in focus 10 to 20 μm shallower than the cones. In fact, when the rods are in focus, the cones typically show a complex irregular intensity profile that can mislead both researchers and automated cell counting algorithms into identifying cones as rod clusters. The dark ring characteristic of cone photoreceptors at eccentricities larger than 5°–10° is not always distinct enough to confidently identify each cone as such (see Fig. 7). It can be seen in the sequence of images in Fig. 7 that the complex intensity profiles corresponding to large cone photoreceptors vary with focus, and in fact, more rapidly than the rod photoreceptor mosaic. This suggests that these patterns might be artifactual, but more experiments following the mosaic over time, using light sources with various wavelengths and coherence lengths, as well as pinhole sizes, need to be performed to determine their nature.

From the practical point of view, cones can be disambiguated from rods by recording two images at each retinal location, one with each of the photoreceptor mosaics in focus. While combining images taken over extended time periods also results in improved visualization of the rod and cone mosaics, this technique would be impractical for routine imaging of patients.

Axial intensity profiles of the cone and rod mosaics estimated from image sequences such as the one in Fig. 7 (shown in Fig. 8) indicate that the rods are brightest 10 to 20 μm shallower than the cones at eccentricities greater than 8°. This is consistent with our qualitative observation of rods appearing in focus shallower than the cones. It is also worth noting that despite the inferior axial resolution of the AOSO (~15 μm) compared with current AO optical coherence tomographs (OCTs) (2–3 μm), the axial intensity profiles suggest two peaks that

#145204 - $15.00 USD Received 1 Apr 2011; revised 2 Jun 2011; accepted 3 Jun 2011; published 8 Jun 2011
(C) 2011 OSA

might correspond to both ends of the cone outer segments [27–29]. If this were indeed the case, the single peak in the axial intensity profile of the rod mosaic would correspond to the interface between the external limiting membrane (ELM) and the rod inner segments (IS). This, however, would be inconsistent with spectral-domain OCT images that show a very faint ELM/IS boundary with respect to the reflections from both ends of the outer segment at all retinal eccentricities (e.g., [27–31].). Further experiments are needed to establish more refined AOSO axial intensity profiles of the cone and rod mosaics at different retinal eccentricities, to clarify the interpretation of the observed axial peaks.

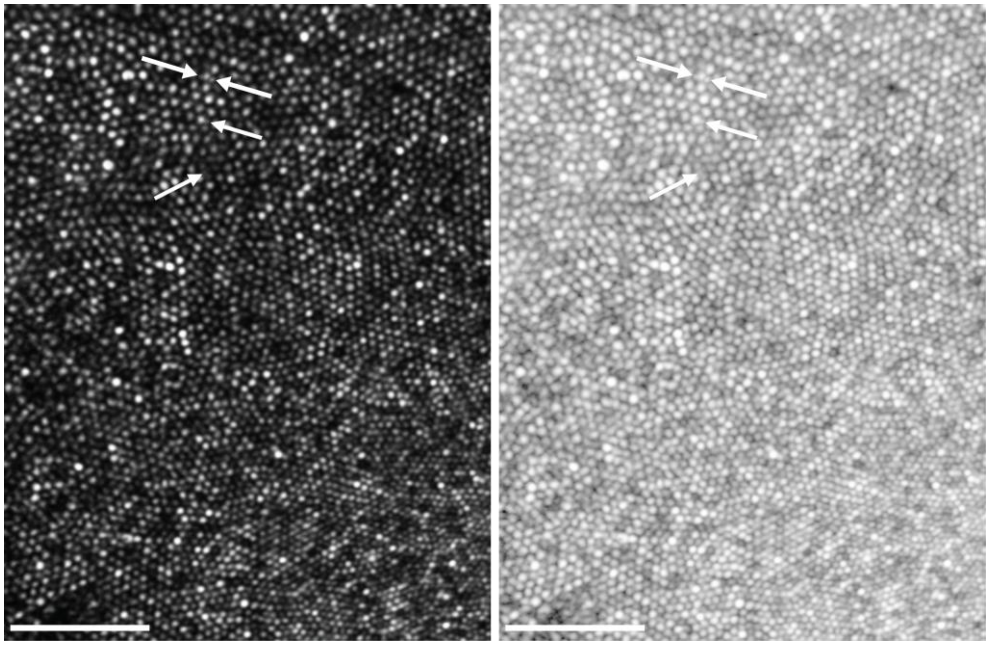

Fig. 6. Reflectance image of the human photoreceptor mosaic from subject JC_0138, collected using 680 nm light and 1.1 Airy disk pinhole size and displayed with linear (*left*) and logarithmic (*right*) gray scale mappings. The image is a montage of two overlapping locations, stitched together using i2k Retina (Dual Align, LLC, Clifton Park, NY, USA). The arrows point to some of the rod photoreceptors closest to the foveal center (significantly smaller than surrounding cones), which is located at the bottom right corner. The scale bars are 50 μm across.

Pinhole sizes between 0.4 and 1.5 Airy disks were used to collect the images for this work in order to explore the 15%–20% lateral resolution benefit that confocal microscopy theory predicts will arise from using sub-Airy disk pinholes [50]. The data collected for this work does not appear to reflect such increase in resolution, although a more exhaustive study is necessary. A plausible explanation for this inconsistency is that the reflective properties of the photoreceptor mosaic are not accurately described by the multiplicative 2D function implied in the mathematical modeling by Wilson and Carlini [50].

Finally, most of the images collected for this study use 680 nm light, although the photoreceptor mosaic can also be resolved with 775 nm light (see Fig. 9), despite the 14% loss of resolution expected due to the longer wavelength. Image contrast when using 680 nm light for imaging is noticeably higher that when using 775 nm light, but the ability to image the photoreceptor mosaic by using infrared light might prove critical when imaging subjects with increased sensitivity to light. Also, note that photoreceptors that appear brighter/darker when imaged with 680 nm light might not necessarily appear so in the 775 nm image and vice versa.

#145204 - $15.00 USD Received 1 Apr 2011; revised 2 Jun 2011; accepted 3 Jun 2011; published 8 Jun 2011
(C) 2011 OSA

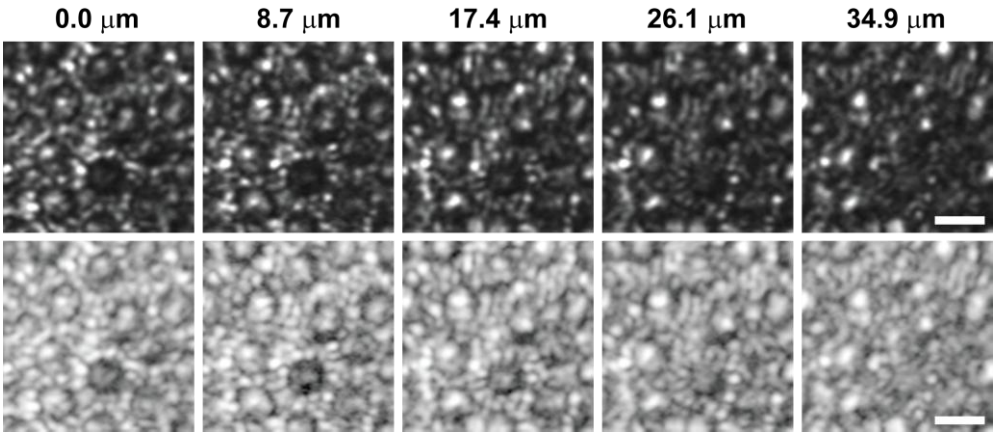


Fig. 7. Reflectance images of the human photoreceptor mosaic from subject DLAB_007 at 10° temporal along the horizontal meridian at different retinal depths, shown with linear (*top row*) and logarithmic (*bottom row*) gray scales. The image series was collected by using 680 nm light and a 0.4 Airy disk pinhole size. The zero depth point indicates the innermost image of the stack, and, thus, increasing values indicate foci closer to the retinal pigment epithelium (RPE). The scale bars are 10 μm across.

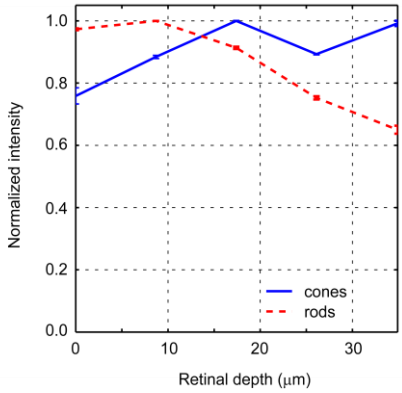


Fig. 8. Axial intensity profiles for the cone and rod photoreceptor mosaics shown in Fig. 7. The (very small) error bars correspond to the errors associated with identifying the boundary of the cones in the images

## 4. Conclusions

We presented the first *in vivo* images of the complete and contiguous rod photoreceptor mosaic in a series of healthy human subjects obtained by using a reflective confocal AOSO. The rod mosaic can be resolved with either 680 or 775 nm light, and often even within single raw frames. The only significant difference between the instrument used for this work and those reported in the bibliography is the simultaneous reduction of astigmatism in pupil and retina conjugate planes [37]. The image registration software used here [38], although critical to increase SNR by averaging multiple frames without introducing significant blur, seems to perform comparably to software used by other researchers [52–55].

Estimates of rod:cone ratio and cell density in the cone and rod photoreceptor mosaics in the 5°–15° eccentricities range imaged for this study are consistent with histological studies, and confirm that we are indeed able to resolve the rod mosaic. Individual rods at the edge of the foveal rod-free zone were observed as close as 190 μm from the foveal center. Qualitative image evaluation and quantitative analysis of axial intensity profiles indicate that the rod

#145204 - $15.00 USD Received 1 Apr 2011; revised 2 Jun 2011; accepted 3 Jun 2011; published 8 Jun 2011
(C) 2011 OSA

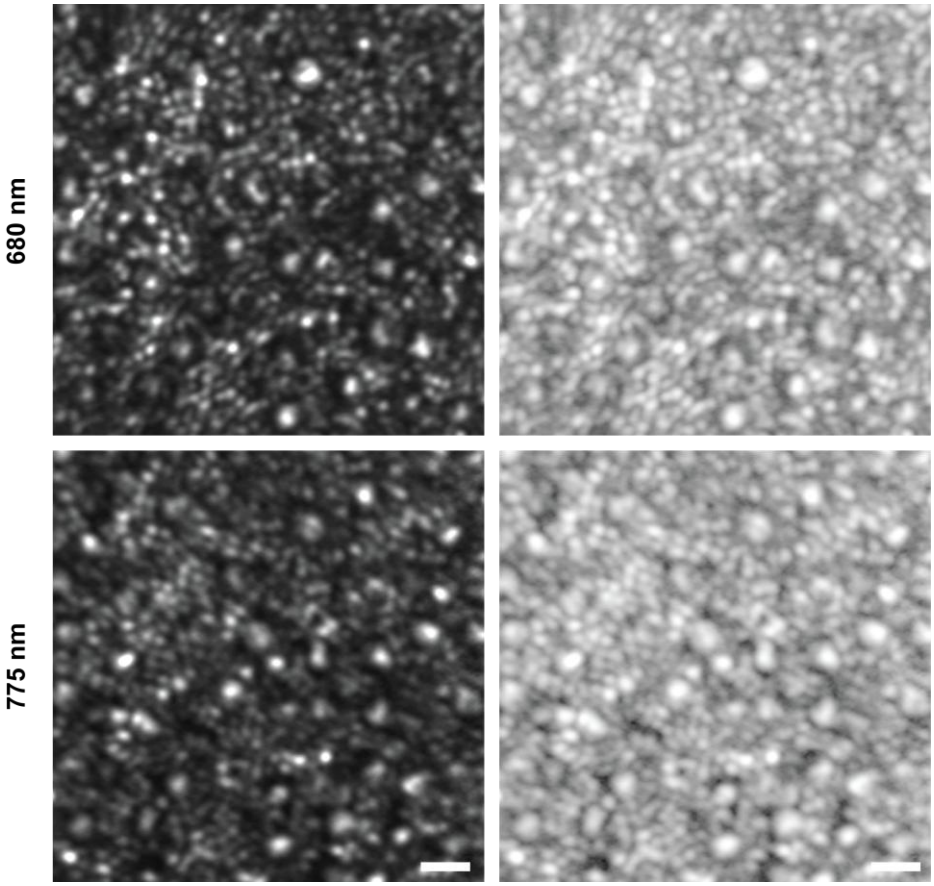


Fig. 9. Reflectance images of the human photoreceptor mosaic collected using 680 and 775 nm light and 1.1 and 1.6 Airy disk pinhole sizes, respectively, shown with linear (left) and logarithmic (right) gray scales. Scale bars are 10 μm across.

mosaic appears in focus 10–20 μm shallower than the cone photoreceptors at retinal eccentricities equal or larger than 8°.

It is worth noting that these results were obtained by using three similarly designed AOSO systems at two different institutions. This represents an important step in the dissemination of AO imaging technology and the use of AO imaging of the photoreceptor mosaic in clinical trials, which typically involves multiple sites. We anticipate that as additional groups acquire the ability to routinely image the rod mosaic, we will see a windfall of important new data on the cellular phenotype in retinal degenerations emerge.

## Acknowledgments

Alfredo Dubra-Suarez, Ph.D., holds a Career Award at the Scientific Interface from the Burroughs Welcome Fund. Joseph Carroll is the recipient of a Career Development Award from Research to Prevent Blindness. This research was supported financially by the National Institutes of Health, Bethesda, Maryland (R01EY014375, P30EY001319, P30EY001931, R01EY017607, and T32EY014537). Funding was also provided by the E. Matilda Ziegler Foundation for the Blind, Hope for Vision, unrestricted grants from Research to Prevent Blindness and the National Science Foundation Science and Technology Center for Adaptive Optics (Santa Cruz, California), managed by the University of California at Santa Cruz (cooperative agreement number AST-9876783). Part of this investigation was conducted in a facility constructed with support from the Research Facilities Improvement Program; from the

National Center for Research Resources, NIH, grant number C06 RR-RR016511. The authors would like to thank Ashavini Pavaskar and Drew Scoles for their assistance with imaging and data processing.

#145204 - $15.00 USD Received 1 Apr 2011; revised 2 Jun 2011; accepted 3 Jun 2011; published 8 Jun 2011
(C) 2011 OSA